Satellite data based abundance mapping of mafic and ultramafic rocks in Mettupalayam, Tamil Nadu, India

Nharakkat Kalarikkal Libeesh[1], Sundaram Arivazhagan[2]

[1] *Centre for Applied Geology, The Gandhigram Rural Institute (Deemed to be University); Gandhigram, Tamil Nadu, India; ORCID ID: 0000-0003-1572-1639*
[2] *Centre for Applied Geology, The Gandhigram Rural Institute (Deemed to be University); Gandhigram, Tamil Nadu, India; e-mail: arivusv@gmail.com (corresponding author), ORCID ID: 0000-0002-6697-660X*

Abstract: The mafic and ultramafic rocks of Mettupalayam belong to the southern granulite terrain of India, which is concomitant with vital economic resources. The advantage of Advanced Spaceborne Thermal Emission and Reflectance Radiometer (ASTER) data for mapping the litho units are exploited well here for differentiating the rock units with the aid of band combination (1, 3, 6), principal component analysis (5, 1, 6) and band ratioed band combination (2/3, 3/2, 1/5 and (9–8)/1, (8–6)/2, and (9–6)/3). As part of the field study, the collection of samples and ground control points were carried out and in addition to that, the generation of laboratory reflectance spectra for samples was achieved. The Spectral Angle Mapper (SAM) and Support Vector Machine (SVM) were performed using ASTER data with the aid of spectra obtained from the laboratory conditions to demarcate the abundance of mafic and ultramafic rocks of the area. The XRF method was used to retrieve the major oxides of the field-collected samples and the spectral absorption characters are validated with it. The results show a vibrant interpretation of the litho units.

Keywords: mafic and ultramafic, ASTER, SAM, SVM, band combination, PCA, BR

INTRODUCTION

Southern Granulite Terrain (SGT), the prime example of high-grade metamorphic terrain situated in southern peninsular India consists of a group of crustal blocks namely Madurai, Trivandrum, Madras, Nilgiri, Salem, and Coorg (Collins et al. 2014, Santosh 2020). The ultramafic and mafic complexes associated with these crustal blocks are considered a major source of economically viable resources (Ashley et al. 2012, Meshram et al. 2014). Numerous studies have been carried out in the Neoarchean high-grade metamorphic terrain of SGT with the mineralogical concepts and had given noteworthy results about the mineral resources of the area (Gopalakrishna et al. 1986, Mohan & Jayananda 1999, Scott et al. 2000). Hence, the ingenuity and evaluation of such kinds of resources are important and there is a need for sophisticated and advanced techniques to map the litho units in a time and cost-effective manner. In this regard, remote sensing can give tremendous results in mapping the abundance of rocks with the integrative techniques of spectral characterization as well as image processing (Abrams & Hook 1995, Duuring et al. 2012). The use of multispectral data from the Landsat series of satellites for Earth observation

triggered the identification of minerals and rocks on the ground through a variety of image processing and spectral characterization techniques. Based on this concept, many satellites have been launched with multispectral and hyperspectral sensors (van der Meer et al. 2012). The different image processing techniques, namely band ratio band combinations, principal component analysis, and minimum noise fraction, have been widely used in the litho boundary delineations using multispectral as well as hyperspectral data (Sabins 1999). Spectral characterization is another important method that uses the spectral response of the mineral content. The absorption is occurred based on the chemical content of the mineral and through characterizing the absorption features, the rocks could be identified and validated with either standard spectral libraries like USGS, JHU,

or developed by the researchers. The pixel purity index and matched filtering are the commonly used method to identify the lithological features (Clark 1999, Arivazhagan & Anbazhagan 2017). The present study aims to identify the abundance of mafic and ultramafic rocks in the Mettupalayam area, based on spectral characterization and image processing methods. The band combination, Spectral Angle Mapper (SAM), and Support Vector Machine (SVM) methods are used to identify the rock units and the representative spectral character was studied using the spectra retrieved from the ASTER satellite image based on the Ground Control Points (GCP). The study area map generated using the Survey of India Toposheet numbers 58 E/3, 58A/15 and 58A/16 with a scale of 1:50,000, which is shown in the Figure 1.
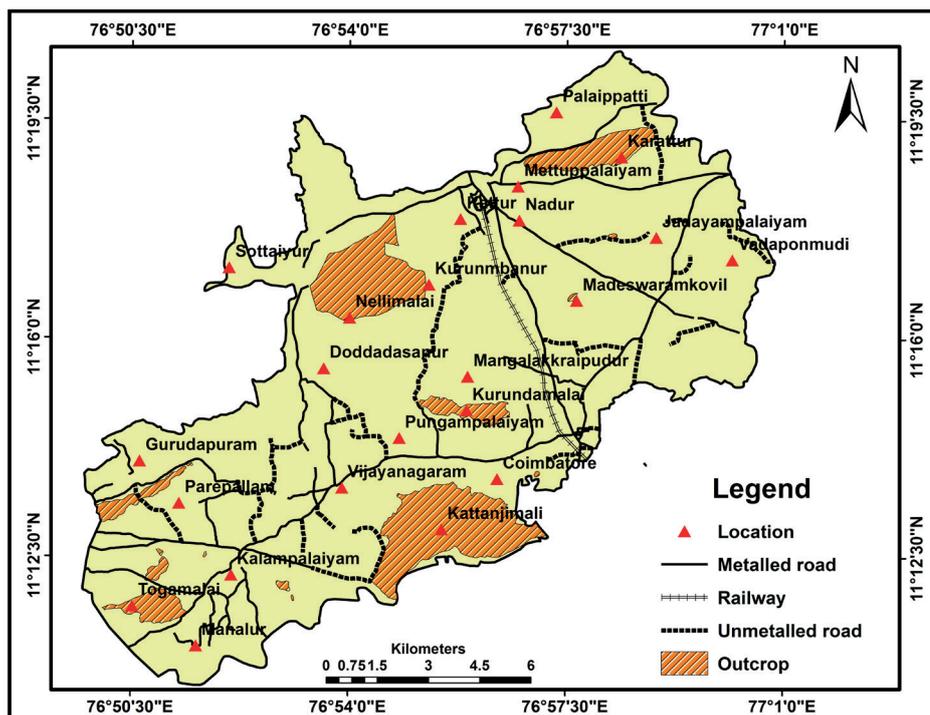
Fig. 1. *Study area map*

GEOLOGY OF THE STUDY AREA

The study area belongs to the Nilgiri block of SGT and comprises charnockite, mafic and ultramafic rocks, and anorthosite (Uthup et al. 2020).

The area underwent different phases of deformation and metamorphism which resulted in the formation of the majority of the rocks in the granulite facies (Chetty & Santosh 2013). As part of the SGT, there are many shear zones identified

and the present study area belongs to the Bhavani shear zone (BSZ) situated between Palghat Cauvery lineament and Moyar – Bhavani lineament (Naganjaneyulu & Harinarayana 2003). The pyroxenite, metagabbro, amphibolite, and meta anorthositic gabbro are the major rock types of the area. The field observations focused on the major four hill rocks, namely Karatur, Karundamalai, Togamalai, and Nellimalai. The Nellimalai was identified with the medium-grained metagabbro whereas Togamalai was with the presence of medium to coarse-grained pyroxenite and medium-grained gabbro. The Karundamalai noted the presence of both fine and medium-grained gabbro and gabbroic anorthosite. The Karatur occurred with the layered complex of pyroxenite and amphibole. The geology map of the area, generated with the reference of map published by the Geological Survey of India, is shown in Figure 2.
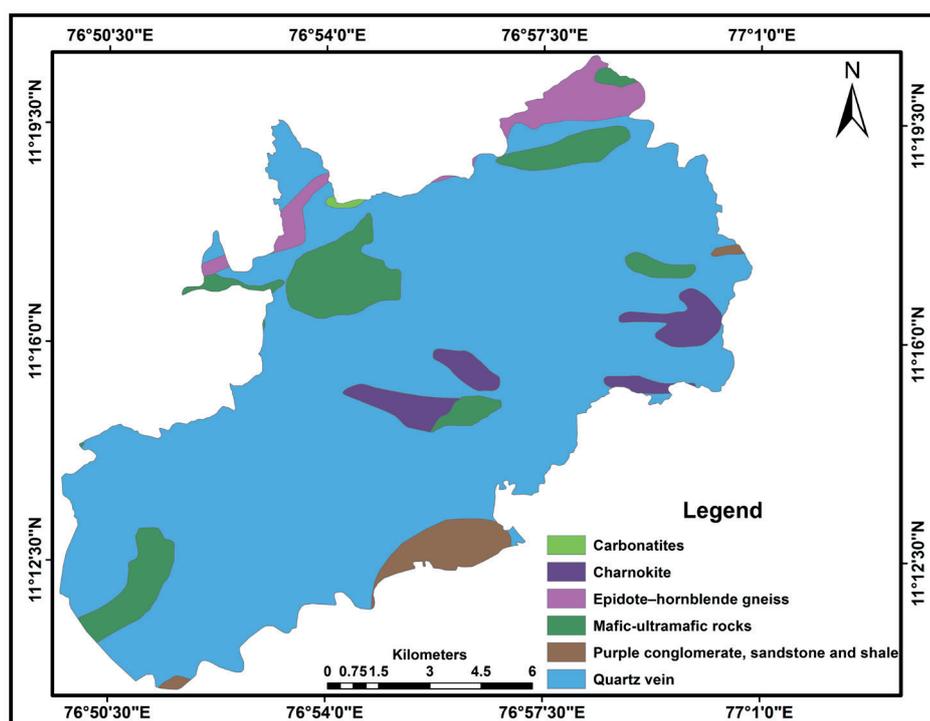
Fig. 2. *Geology map of the area*

MATERIALS AND METHODS

Through fieldwork, the mafic and ultramafic rock samples were collected along with the ground control point (GCP). The atmospherically corrected ASTER data acquisition from the USGS Earth Explorer and the conversion of radiance to reflectance were done using the procedure mentioned by Arivazhagan & Anbazhagan (2017). The first nine bands of ASTER data in the range of the visible and infrared portion of the electromagnetic spectrum are used to generate the band combination. By using the ASD Fieldspec 4 Spectroradiometer the laboratory-based spectra were generated in the wavelength range of 350 nm to 2500 nm using the facility in IIST, Trivandrum. The SAM and SVM were performed to delineate the abundance of rock units. In addition, the satellite-based spectra were obtained and resampled to the lab spectra. The XRF data of the samples were obtained using the facility available at National Centre for Earth Science Studies (NCESS), Trivandrum to find out the major oxides and compare them with the spectral character.

RESULTS AND DISCUSSION

Geochemistry

The 20 field samples collected from the different locations in and around Mettupalayam were scrutinized and three representative samples of mafic and ultramafic were selected. The pyroxenite, metagabbro, and gabbro are the representative samples and Table 1 shows the major oxides percentage of rock types obtained through XRF analysis.

Table 1
Major oxides [wt.%] of the samples

Sample	Pyroxenite	Gabbro	Metagabbro
SiO_2	47.73	49.57	52.80
TiO_2	0.69	0.97	0.60
Al_2O_3	13.43	15.91	13.30
MnO	0.33	0.19	0.20
Fe_2O_3	15.44	10.50	10.40
CaO	13.08	14.58	11.70
MgO	6.71	5.39	6.41
Na_2O	0.92	2.03	3.15
K_2O	0.04	0.08	0.60
P_2O_5	0.11	0.27	0.10

Band combinations

Objects on the ground have different reflectance properties based on their color, structure, texture, etc. Satellite data records such kinds of objects and it can be utilized in many kinds of studies (Gupta 2003). The basic filters, namely red, green and blue, can give better discrimination of features by allocating different bands to them. Different band combinations can be generated and they can be well suited for the identification of rocks, minerals, vegetation, etc. (Gomez et al. 2005, Libeesh et al. 2021). Based on the spectral behavior, various band combinations were derived for mafic and ultramafic rocks. Among that, bands 1, 3, and 6 were more suitable for demarcating the boundary of litho units. From the selected bands, the highest reflectance is found in the band 1 of ASTER,

against an absorption at 600 nm in red bands corresponding to the VNIR. This kind of absorption is due to the presence of ferrous ion. The spectral signature extracted from the ASTER sensor for band 3 and 6, which is also characterized by the low absorption at 860 nm and 2225 nm, assigned to the green and blue band can be related to the presence of Fe^{2+} in pyroxene and Al-OH. Hence this combination is more adequate and the generated image shows the mafic and ultramafic litho units in rose color (Fig. 3).

Principal Component Analysis (PCA)

Principal Component Analysis (PCA) is an image enhancement technique used to utilize the maximum spectral contrast of all bands of multispectral data, and it is more reliable than the original image (Anbazhagan et al. 2012, Arivazhagan & Anbazhagan 2017). In another sense, PCA is a statistical analysis approach used to reduce irradiance in the bands, so each band can represent particular features, and a combination of this can be interpreted as more valuable information (Ge et al. 2018). Considering the PC bands, the PC1, PC2, and PC3 are more informative than other PC bands since 98% spectral information is contained in these three bands (Gupta 2003). PCA is a common and well-known technique in the field of lithological mapping (Moore et al. 2008, Liu et al. 2014). The visual interpretation to the lithological mapping is meant to discriminate the features by means of the color composite image and in many cases, the color composites are not very meaningful because the PC image is dependent on transform coefficient (Yamaguchi & Naito 2003). In the present study, PCA was applied to all 9 bands of ASTER data ranges in the visible & infrared region to highlight the lithological interference. Most of the studies used PC 245, PC 542, PC 754, and PC 376 combinations to demarcate the lithological features (Guha et al. 2015, Pour et al. 2019). Among the various PC band combinations generated for the area, this study utilizes the band combinations of PC 516 (Fig. 4) to delineate the mafic and ultramafic lithology. The band combination of 516 depicts mafic-ultramafic rocks in a green color.
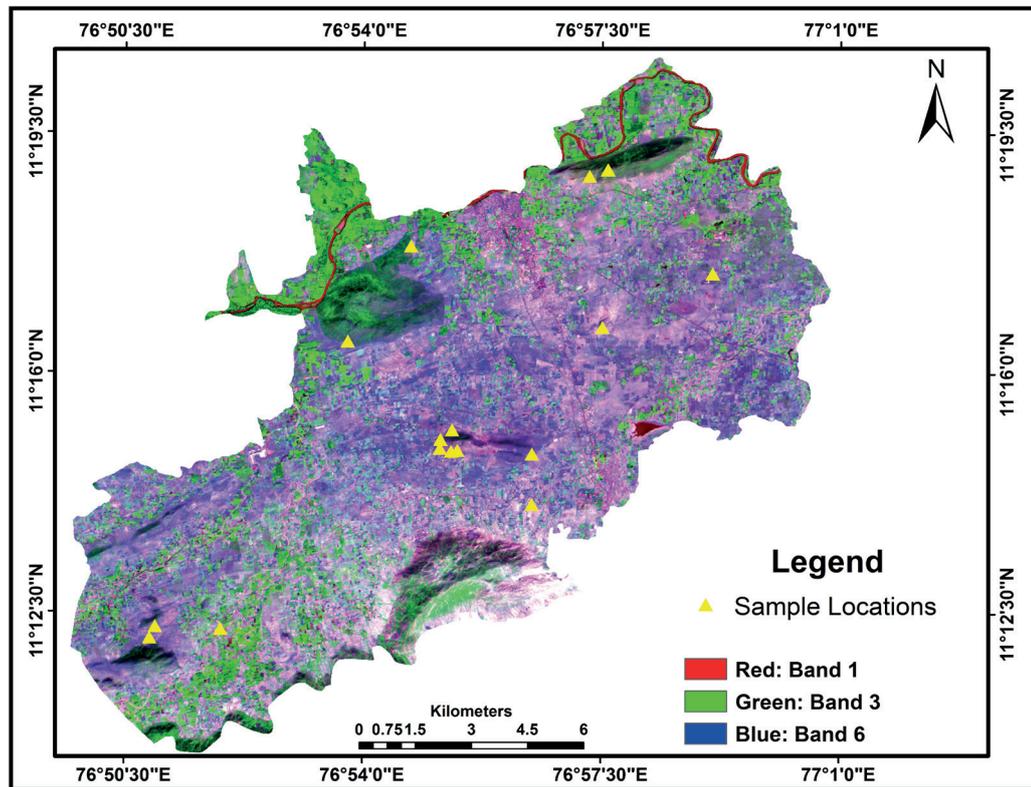
Fig. 3. *The band combination generated using ASTER bands 1, 3, and 6 and mafic and ultramafic rocks enhanced in the rose color*
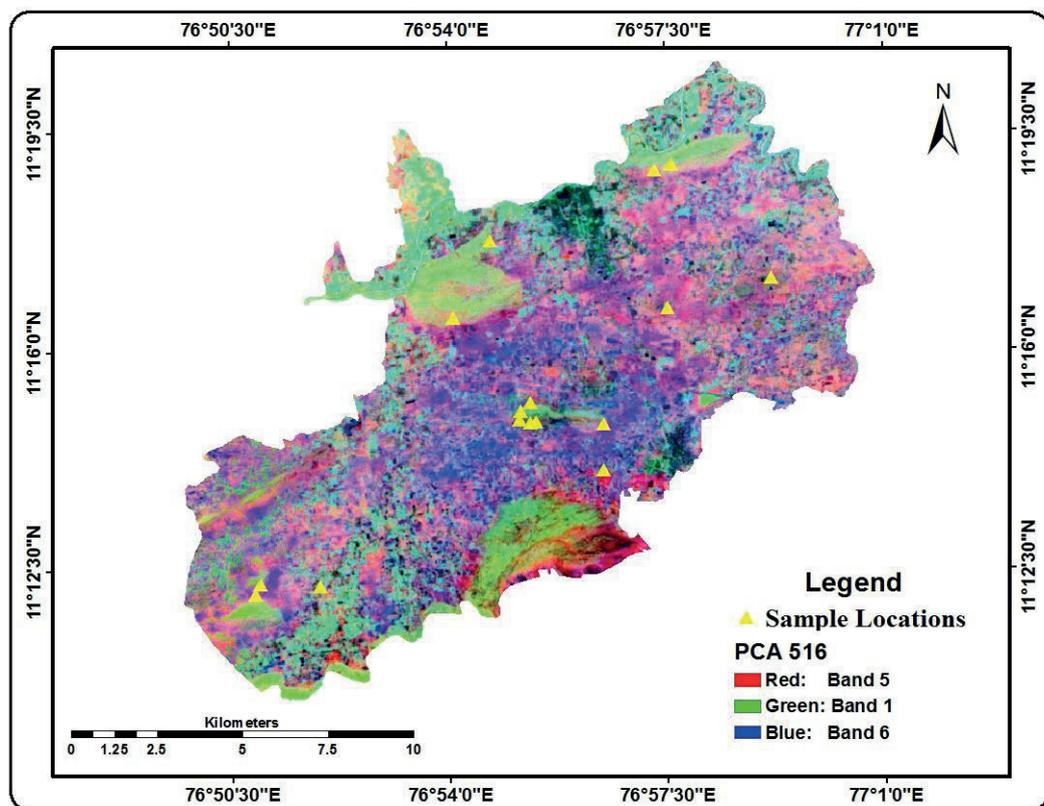
Fig. 4. *Principal component analysis with ASTER 5, 1, 6 bands under red, green, and blue filters. Mafic-ultramafic complexes are enhanced in green color*

Band Ratio (BR)

Different bands hold different spectral characters and their proper combination can make the image more informative as well as more compactable to analyze the features (Hewson et al. 2005, Gad & Kusky 2007). BR is a generalized statistical technique performed by dividing two different bands into a single band which increases the spectral difference between the bands and it would help more to demarcate the lithology (Pour & Hashim 2015, Emam et al. 2016). The bands are aligned in the red, green, and blue filters as the principal colors based on spectral characters, and it is more utilized by the combination of shortwave and longwave bands (Ibrahim et al. 2016). Considering the spectral information of visible and infrared portions, ASTER data can have more application in the BR due to its spectral as well as spatial characters (Mars & Rowan 2011, Rajendran et al. 2012). Concerning the lithology, many combinations were derived to demarcate the lithology, such as the ratio of 5/7, 4/5, and 3/1 for the ETM+ data used to delineate the mafic and ultramafic rocks (Khan & Mahmood 2008). 4/7, 4/5, and 4/1 of ASTER data was made use of to discriminate the ophiolite lithology by Pournamdari & Hashim (2014). Another study by Liu et al. (2014) shows that 2/1, 5/4, and 6/8 are more useful to map the mafic and ultramafic rocks. BR 5/7, 5/1 and 5/4 × 4/3 (Sultan et al. 1987), 3/5, 3/1 and 5/7 (Sabins 1999), 5/3, 5/1, 7/5 and 7/5, 5/4 and 3/1 (Gad & Kusky 2007) are some more examples used in the mapping of mafic and ultramafic lithological units.

Based on the spectral behavior, various band ratioed combinations were derived for the mafic and ultramafic rocks. Among that, bands 2/3, 3/2, 1/5 were more suitable for demarcating the boundary of litho units. From the selected bands, the highest reflectance is found in the band 1/5 of ASTER, against an absorption at 1200 nm in blue bands corresponding to the SWIR. This kind of absorption is due to the presence of ferrous ion. The spectral signature extracted from the ASTER sensor for bands 2/3 and 3/2, which is also characterized by the low absorption at 1200 nm and 810 nm, assigned to the red and green band can be related to the presence of Fe^{2+} in plagioclase and pyroxene respectively. Hence this combination is more adequate and the generated image shows the mafic and ultramafic litho units in a light blue color (Fig. 5).

The suppression of the spectral character was done using the band ratioed band combination (9–8)/1, (8–6)/2, and (9–6)/3, in that, the higher reflectance is noted in the (9–6)/3, against the Mg-OH absorption at 2300 nm in the blue band. The spectral signature extracted from the ASTER bands (9–8)/1 and (8–6)/2, now have lower reflectance due to the ferrous iron present in 1200 nm and 1800 nm respectively. Hence, the band combination of (9–8)/1, (8–6)/2, and (9–6)/3 shows the mafic and ultramafic rocks in a sky blue color (Fig. 6).

Spectral Angle Mapper (SAM)

Spectral Angle Mapper (SAM) is an advanced mapping technique which uses spectral similarities of features through the n-D angle between reference spectra to the similar pixels (Arivazhagan & Anbazhagan 2017). It is an algorithm based process that calculates the angle of two spectra to determine the similarity by considering it as a vector in space with an equal extent of the bands present in it (Bishop et al. 2011). While using the calibrated reflectance spectra can be oblivious to the albedo effects and illumination (Arivazhagan & Anbazhagan 2017). The ASCII file from the spectral library, laboratory conditions or satellite image is used as the endmember spectra and the angle was determined to the reference spectrum vector to the targeted pixels vector in n-D space (Elsaid et al. 2014). The small-angle represent a high resemblance where the large angle will not be considered and most of the study shows 90 to 95 percent accuracy (Othman & Gloaguen 2014). In the present study, rock units are characterized by using the SAM method by taking laboratory spectra as reflectance spectra (Fig. 7A). The red color shows the abundance of mafic and ultramafic rocks. Afterward, it is overlaid with a band combination (Fig. 7B) and the represented spectra were generated using GCP.
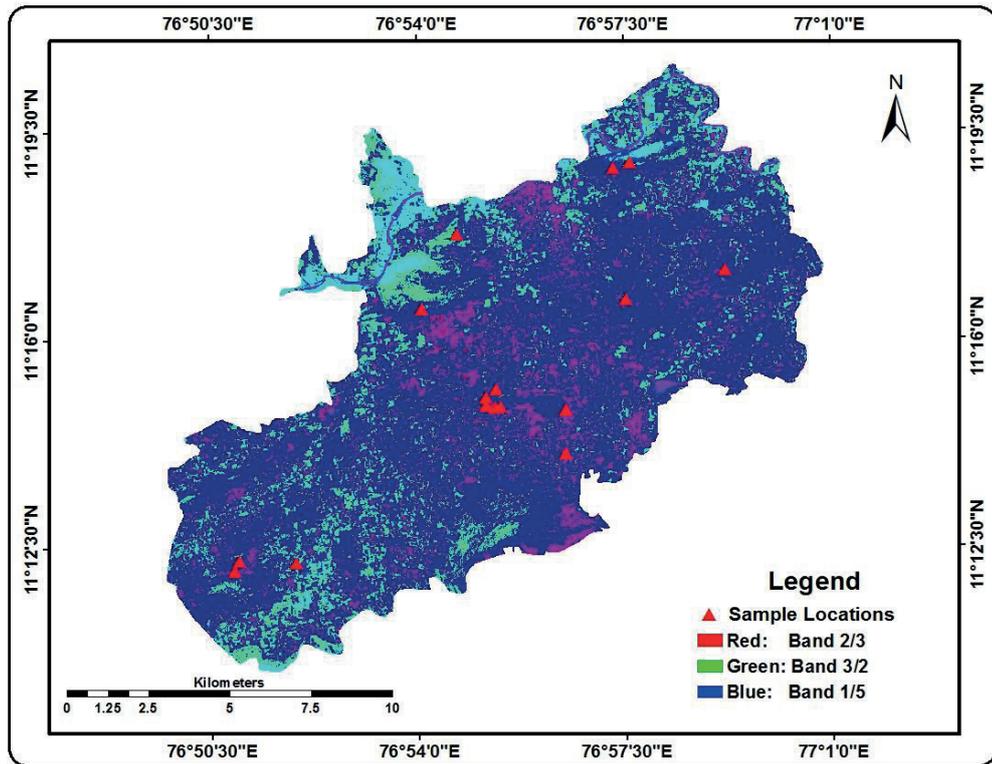
Fig. 5. *ASTER band radioed band combination for mafic-ultramafic complexes with 2/3, 3/2, 1/5 RGB image enhanced the mafic-ultramafic complexes in light blue color*
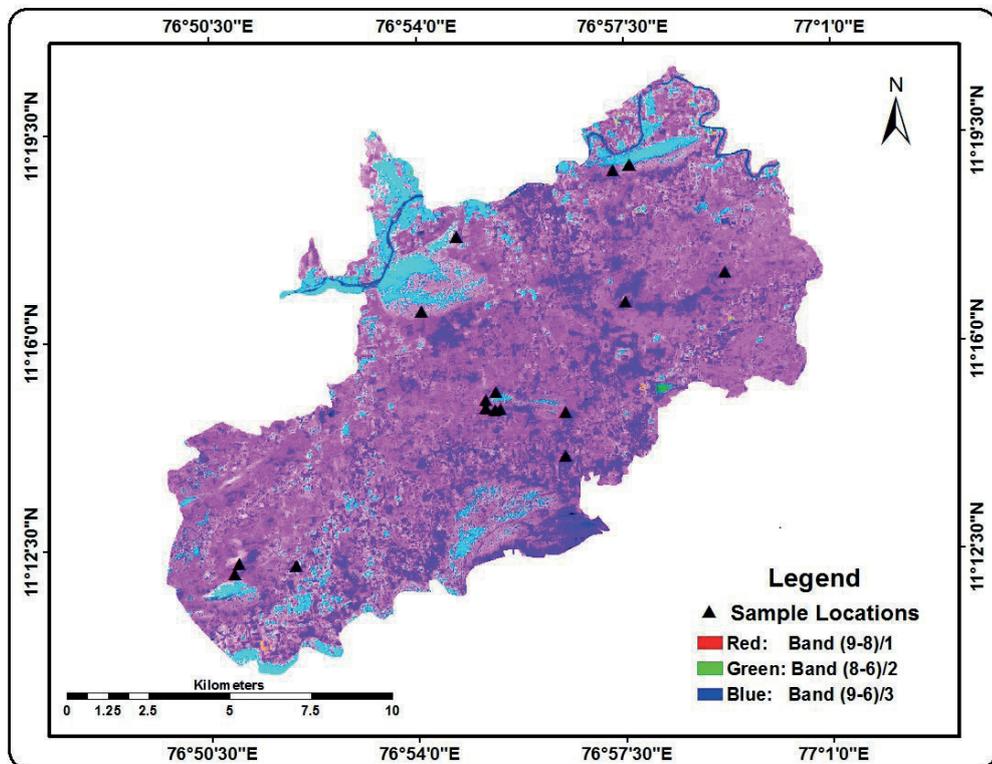
Fig. 6. *ASTER band radioed band combination for mafic-ultramafic complexes with (9–8)/1, (8–6)/2, and (9–6)/3 RGB image enhanced the mafic-ultramafic complexes in sky blue color*

Spectral characterization

Reflectance spectral profiling is a widely used method to prospect minerals associated with the ground (Goetz 1992). The reflected or scattered lights from the object of consideration records the features, especially chemical content, as a function of wavelength (Clark & Roush 1984). The visible and infrared portions of electromagnetic radiation utilized to identify the minerals and the vibrational and electronic process are the major factor in the absorption features of the spectra (Sgavetti et al. 2006). The three rocks samples show major absorption in the wavelengths of 650 nm, 900 nm, 2250 nm, and 2300 nm due to the presence of Fe^{3+}, OPx, Al-OH, and Mg-OH respectively (Fig. 7C). The spectra taken from the image based on the GCP show the major absorptions at 650 nm, 850 nm, 2150 nm and 2300 nm

(Fig. 7D). While considering it, all the absorptions identified in the lab spectra could be seen in the image spectra as well. The detailed spectral absorption and its causes are listed in Table 2.

Table 2
Spectral absorptions and their causes

SI No.	Absorption range [nm]	Cause
1	650	ferric ion
2	850–900	OPx
3	1100	CPx
4	1200	FeO absorption
5	1450–1650	ferric ion
6	1750–1950	ferrous ion
7	2150	Al-OH absorption
8	2300	Mg-OH vibration spectra
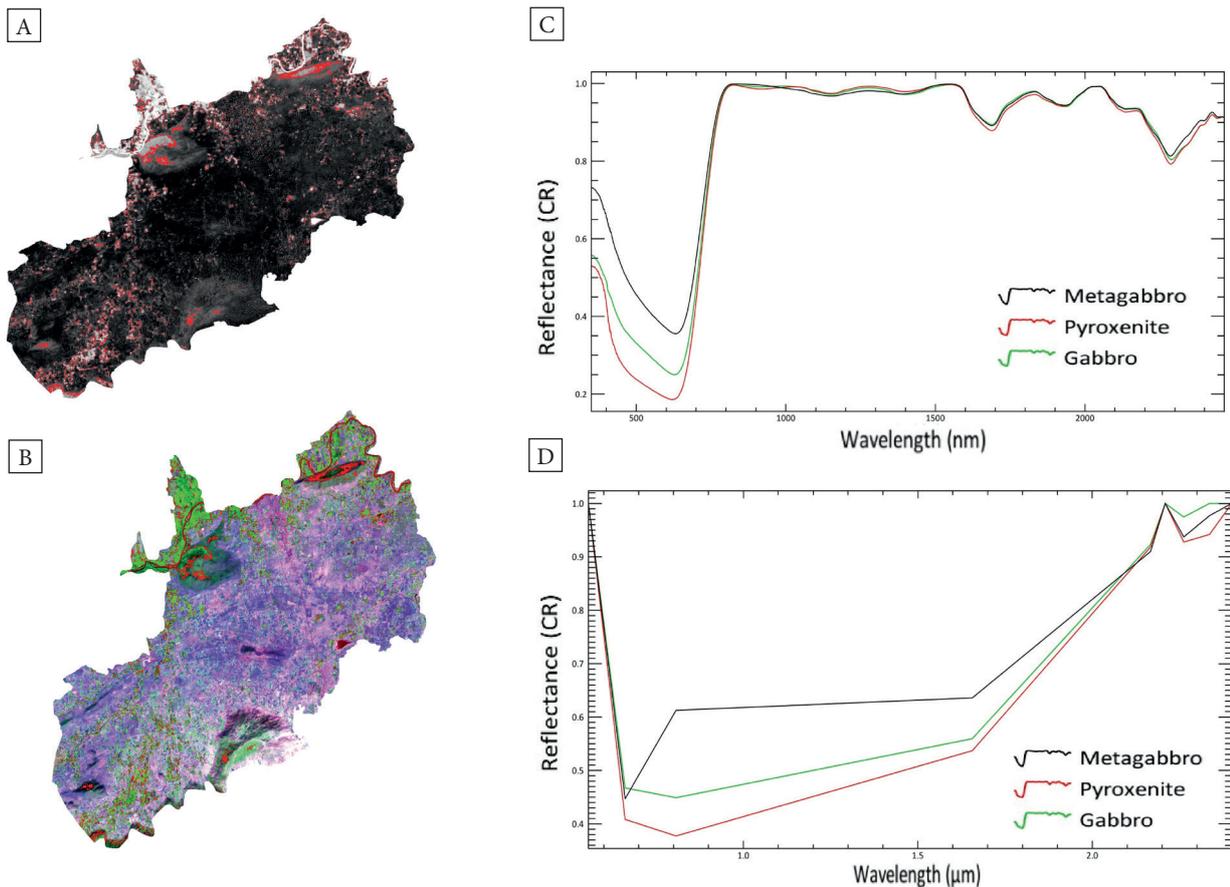
Fig. 7. *The mafic and ultramafic abundance map of the area retrieved from SAM and red color indicating the abundance of the mafic and ultramafic rock types (A). The result from SAM overlaid to the band combination generated using ASTER bands 1, 3, and 6 (B). The reflectance spectra were taken at laboratory conditions (C). The ASTER spectra were obtained from the image using the GCP (D)*

Support Vector Machine (SVM)

This is a supervised classification technique developed based on a statistical approach with the ability to process small datasets in a higher accuracy classification (Vapnik 2000, Mantero et al. 2005, Mountrakis et al. 2011). The SVM designs a linear hyperplane to separate the classes with the help of known classes dataset (Bishop et al. 2011, Gasmi et al. 2016). The optimally separating hyperplane focuses on the known classes, and based on the newer data classification takes place (Smirnoff et al. 2008, Bahari et al. 2014). With the ability to generate good quality classifications, SVM has mostly been used in lithological mapping (Guha et al. 2019) and it enables the discrimination of ore, volcanic and sedimentary rocks in the field with more than 95 percent accuracy (Abedi et al. 2012, Othman & Gloaguen 2014, Adiri et al. 2016).

The classification of features was done for the area mainly with four classes, namely litho units, cultivation, build-up area, and water body (Fig. 8).

The training samples were marked out from the satellite data and the SVM was performed using this, while the GCP collected from the field was used to identify the correct features. Based on the classification, litho units are indicated by a yellow color, the cultivation land was marked in green, built-up areas in blue and water bodies were designated by a red color.

CONCLUSION

The present study aims to map the abundance of mafic-ultramafic rocks, namelythe pyroxenite, gabbro, and metagabbro of the Mettupalayam area using the various image processing techniques as well as the characterization of spectral behavior. The ASTER multispectral data with the first nine bands were utilized in this study. The band combination (1, 3, 6), principal component analysis (5, 1, 6), and band ratioed band combination (2/3, 3/2, 1/5 and (9–8)/1, (8–6)/2, and (9–6)/3) are generated and well suitable for demarcating the boundaries.
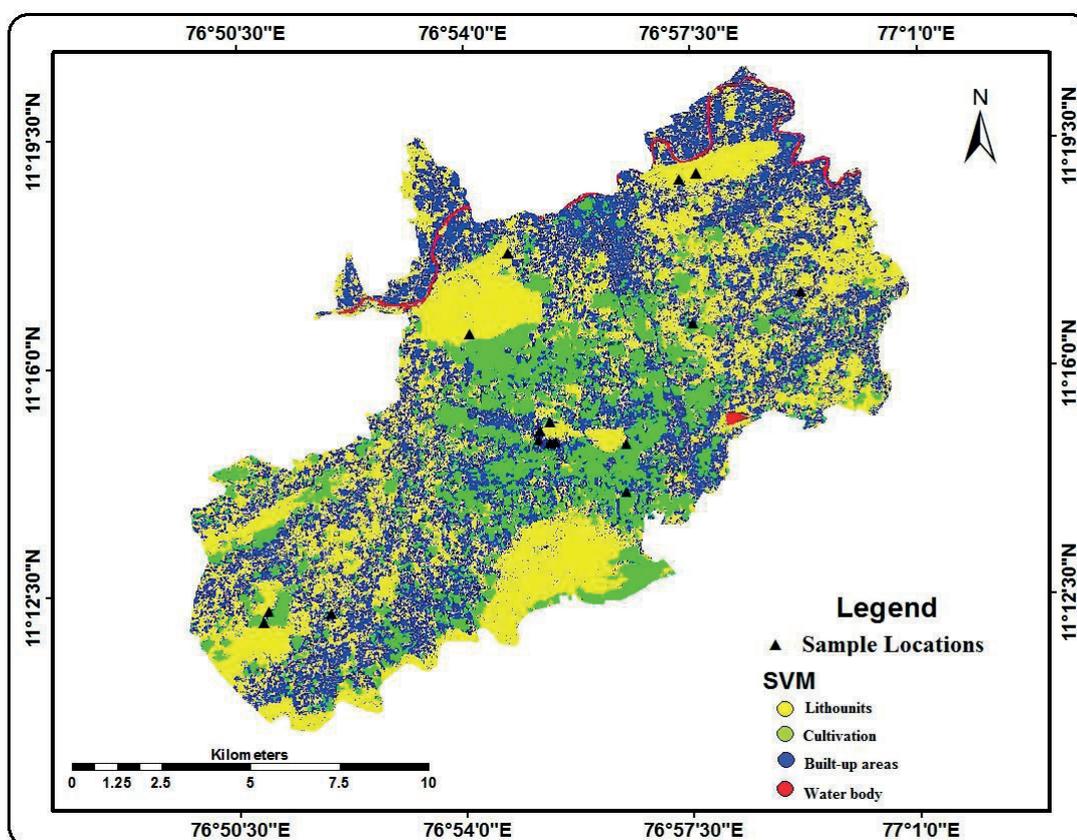
Fig. 8. *SVM for the study area with four classes*

The subpixel classification to retrieve the abundance of the litho units were performed using SAM, with reference to the lab spectra that were depicted valuable information through the map as well as the spectral aspects. The SVM method provides accurate results to classify different litho units with the advantage of reflectance spectral characteristics. The use of higher spectral and spatial resolution could make it more accurate and this will be conducted in the near future.

REFERENCES

Abedi M., Norouzi G.-H. & Bahroudi A., 2012. Support vector machine for multi-classification of mineral prospectivity areas. *Computers & Geosciences*, 46, 272–283. https://doi.org/10.1016/j.cageo.2011.12.014.

Abrams M. & Hook S.J., 1995. Simulated Aster Data for Geologic Studies. *IEEE Transactions on Geoscience and Remote Sensing*, 33(3), 692–699. https://doi.org/10.1109/ 36.387584.

Adiri Z., El Harti A., Jellouli A., Maacha L. & Bachaoui E.M., 2016. Lithological mapping using Landsat 8 OLI and Terra ASTER multispectral data in the Bas Drâa inlier, Moroccan Anti Atlas. *Journal of Applied Remote Sensing*, 10(1), 016005. https://doi.org/10.1117/1.JRS.10.016005.

Anbazhagan S., Sainaba N.K. & Arivazhagan S., 2012. Remote Sensing Study of Sittampundi Anorthosite Complex, India. *Journal of the Indian Society of Remote Sensing*, 40, 145–153. https://doi.org/10.1007/s12524-011-0126-y.

Arivazhagan S. & Anbazhagan S., 2017. ASTER Data Analyses for Lithological Discrimination of Sittampundi Anorthositic Complex, Southern India. *Geosciences Research*, 2(3), 196–209. https://doi.org/10.22606/gr.2017.23005.

Ashley P., Craw D., Mackenzie D., Rombouts M. & Reay A., 2012. Mafic and ultramafic rocks, and platinum mineralisation potential, in the Longwood Range, Southland, New Zealand. *New Zealand Journal of Geology and Geophysics*, 55, 3–19. https://doi.org/10.1080/00288306.2011.623302.

Bahari N.I.S., Ahmad A. & Aboobaider B.M., 2014. Application of support vector machine for classification of multispectral data. *IOP Conference Series: Earth and Environmental Science*, 20, 012038. https://doi.org/10.1088/1755-1315/20/1/012038.

Bishop C.A., Liu J.G. & Mason P.J., 2011. Hyperspectral remote sensing for mineral exploration in Pulang, Yunnan province, China. *International Journal of Remote Sensing*, 32, 2409–2426. https://doi.org/10.1080/01431161003698336.

Chetty T.R.K. & Santosh M., 2013. Proterozoic orogens in southern Peninsular India: Contiguities and complexities. *Journal of Asian Earth Sciences*, 78, 39–53. https://doi.org/10.1016/j.jseaes.2013.02.021.

Clark R.N., 1999. Spectroscopy of Rocks and Minerals and Principles of Spectroscopy. [in:] Rencz A.N. (ed.), *Manual of Remote Sensing, Volume 3, Remote Sensing for The Earth Sciences*, Wiley, 3–58.

Clark R.N. & Roush T.L., 1984. Reflectance spectroscopy: quantitative analysis techniques for remote sensing applications. *Journal of Geophysical Research*, 89, 6329–6340. https://doi.org/10.1029/JB089IB07P06329.

Collins A.S., Clark C. & Plavsa D., 2014. Peninsular India in Gondwana: The tectonothermal evolution of the Southern Granulite Terrain and its Gondwanan counterparts. *Gondwana Research*, 25, 190–203. https://doi.org/10.1016/j.gr.2013.01.002.

Duuring P., Hagemann S.G., Novikova Y., Cudahy T. & Laukamp C., 2012. Targeting iron ore in banded iron formations using ASTER data: Weld Range greenstone belt, Yilgarn craton, Western Australia. *Economic Geology*, 107, 585–597. https://doi.org/10.2113/econgeo.107.4.585.

Elsaid M., Aboelkhair H., Dardier A., Hermas E. & Minoru U., 2014. Processing of Multispectral ASTER Data for Mapping Alteration Minerals Zones: As an Aid for Uranium Exploration in Elmissikat-Eleridiya Granites, Central Eastern Desert, Egypt. *The Open Geology Journal*, 8, 69–83. https://doi.org/10.2174/1874262901408010069.

Emam A., Zoheir B. & Johnson P., 2016. ASTER-based mapping of ophiolitic rocks: Examples from the Allaqi-Heiani suture, SE Egypt. *International Geology Review*, 58, 525–539. https://doi.org/10.1080/00206814.2015.1094382.

Gad S. & Kusky T., 2007. ASTER spectral ratioing for lithological mapping in the Arabian-Nubian shield, the Neoproterozoic Wadi Kid area, Sinai, Egypt. *Gondwana Research*, 11, 326–335. https://doi.org/10.1016/j.gr.2006.02.010.

Gasmi A., Gomez C., Zouari H., Masse A. & Ducrot D., 2016. PCA and SVM as geo-computational methods for geological mapping in the southern of Tunisia, using ASTER remote sensing data set. *Arabian Journal of Geosciences*, 9, 1–12. https://doi.org/10.1007/s12517-016-2791-1.

Ge W., Cheng Q., Jing L., Armenakis C. & Ding H., 2018. Lithological discrimination using ASTER and Sentinel-2A in the Shibanjing ophiolite complex of Beishan orogenic in Inner Mongolia, China. *Advances in Space Research*, 62, 1702–1716. https://doi.org/10.1016/j.asr.2018.06.036.

Goetz A.F.H., 1992. Imaging spectrometry for Earth remote sensing. *Imaging Spectroscopy*, 228, 1147–1153. https://doi.org/10.1126/science.228.4704.1147.

Gomez C., Delacourt C., Allemand P., Ledru P. & Wackerle R., 2005. Using ASTER remote sensing data set for geological mapping, in Namibia. *Physics and Chemistry of the Earth*, 30, 97–108. https://doi.org/10.1016/j.pce.2004.08.042.

Gopalakrishna D., Hansen E.C., Janardhan A.S. & Newton R.C., 1986. The southern high-grade margin of the Dharwar craton. *Journal of Geology*, 94, 247–260. https://doi.org/10.1086/629026.

Guha A., Ghosh B., Vinod Kumar K. & Chaudhury S., 2015. Implementation of reflection spectroscopy based new ASTER indices and principal components to delineate chromitite and associated ultramafic-mafic complex in parts of Dharwar Craton, India. *Advances in Space Research*, 56, 1453–1468. https://doi.org/10.1016/j.asr.2015.06.043.

Guha A., Vinod Kumar K., Porwal A., Rani K., Sahoo K.C., Aneesh Kumar S.R., Singaraju V., Singh R.P., Khandelwal M.K., Raju P.V. & Diwakar P.G., 2019. Reflectance spectroscopy and ASTER based mapping of rock-phosphate in parts of Paleoproterozoic sequences of Aravalli group of rocks, Rajasthan, India. *Ore Geology Reviews*, 108, 73–87. https://doi.org/10.1016/j.oregeorev.2018.02.021.

Gupta R.P., 2003. *Remote Sensing Geology*. Springer Berlin Heidelberg.

Hewson R.D., Cudahy T.J., Mizuhiko S., Ueda K. & Mauger A.J., 2005. Seamless geological map generation using ASTER in the Broken Hill-Curnamona province of Australia. *Remote Sensing of Environment*, 99, 159–172. https://doi.org/10.1016/j.rse.2005.04.025.

Ibrahim W.S., Watanabe K. & Yonezu K., 2016. Structural and litho-tectonic controls on Neoproterozoic base metal sulfide and gold mineralization in North Hamisana shear zone, South Eastern Desert, Egypt: The integrated field, structural, Landsat 7 ETM + and ASTER data approach. *Ore Geology Reviews*, 79, 62–77. https://doi.org/10.1016/j.oregeorev.2016.05.012.

Khan S.D. & Mahmood K., 2008. The application of remote sensing techniques to the study of ophiolites. *Earth-Science Reviews*, 89, 135–143. https://doi.org/10.1016/j.earscirev.2008.04.004.

Libeesh N.K., Naseer K.A., Arivazhagan S., Abd El-Rehim A.F., Mahmoud K.A., Sayyed M.I. & Khandaker M.U., 2021. Advanced nuclear radiation shielding studies of some mafic and ultramafic complexes with lithological mapping. *Radiation Physics and Chemistry*, 189, 109777. https://doi.org/10.1016/j.radphyschem.2021.109777.

Liu L., Zhou J., Jiang D., Zhuang D. & Mansaray L.R., 2014. Lithological discrimination of the mafic-ultramafic complex, Huitongshan, Beishan, China: Using ASTER data. *Journal of Earth Science*, 25, 529–536. https://doi.org/10.1007/s12583-014-0437-3.

Mantero P., Moser G. & Serpico S.B., 2005. Partially Supervised classification of remote sensing images through SVM-based probability density estimation. *IEEE Transactions on Geoscience and Remote Sensing*, 43, 559–570. https://doi.org/10.1109/TGRS.2004.842022.

Mars J.C. & Rowan L.C., 2011. ASTER spectral analysis and lithologic mapping of the Khanneshin carbonatite volcano, Afghanistan. *Geosphere*, 7, 276–289. https://doi.org/10.1130/GES00630.1.

van der Meer F.D., van der Werff H.M.A., van Ruitenbeek F.J.A., Hecker C.A., Bakker W.H., Noomen M.F., van der Meijde M., Carranza E.J.M., de Smeth J.B. & Woldai T., 2012. Multi- and hyperspectral geologic remote sensing: A review. *International Journal of Applied Earth Observation and Geoinformation*, 14, 112–128. https://doi.org/10.1016/j.jag.2011.08.002.

Meshram T.M., Nannaware S.B., Bhatacharjee S., Waghmare M.M. & Rajakumar T., 2014. PGE distribution in the Chromite bearing mafic-ultramafic Kondapalli Layered Complex, Krishna district, Andhra Pradesh, India. *Open Geosciences*, 7, 252–263. https://doi.org/10.1515/geo-2015-0018.

Mohan A. & Jayananda M., 1999. Metamorphism and Isotopic Evolution of Granulites of Southern India: Reference to Neoproterozoic Crustal Evolution. *Gondwana Research*, 2, 251–262. https://doi.org/10.1016/S1342-937X(05)70149-0.

Moore F., Rastmanesh F., Asadi H. & Modabberi S., 2008. Mapping mineralogical alteration using principal-component analysis and matched filter processing in the Takab area, north-west Iran, from ASTER data. *International Journal of Remote Sensing*, 29, 2851–2867. https://doi.org/10.1080/01431160701418989.

Mountrakis G., Im J. & Ogole C., 2011. Support vector machines in remote sensing: A review. *ISPRS Journal of Photogrammetry and Remote Sensing*, 66, 247–259. https://doi.org/10.1016/j.isprsjprs.2010.11.001.

Naganjaneyulu K. & Harinarayana T., 2003. Evidence for continent-continent collision zone in the South Indian Shield region. *Gondwana Research*, 6, 902–911. https://doi.org/10.1016/S1342-937X(05)71034-0.

Othman A.A. & Gloaguen R., 2014. Improving lithological mapping by SVM classification of spectral and morphological features: The discovery of a new chromite body in the Mawat ophiolite complex (Kurdistan, NE Iraq). *Remote Sensing*, 6, 6867–6896. https://doi.org/10.3390/rs6086867.

Pour A.B. & Hashim M., 2015. Hydrothermal alteration mapping from Landsat-8 data, Sar Cheshmeh copper mining district, south-eastern Islamic Republic of Iran. *Journal of Taibah University for Science*, 9, 155–166. https://doi.org/10.1016/j.jtusci.2014.11.008.

Pour A.B., Park Y., Crispini L., Läufer A., Hong J.K., Park T.-Y.S., Zoheir B., Pradhan B., Muslim A.M., Hossain M.S. & Rahmani O., 2019. Mapping listvenite occurrences in the damage zones of Northern Victoria Land, Antarctica using ASTER satellite remote sensing data. *Remote Sensing*, 11(12), 1408. https://doi.org/10.3390/rs11121408.

Pournamdari M. & Hashim M., 2014. Detection of chromite bearing mineralized zones in Abdasht ophiolite complex using ASTER and ETM+ remote sensing data. *Arabian Journal of Geosciences*, 7, 1973–1983. https://doi.org/10.1007/s12517-013-0927-0.

Rajendran S., al-Khirbash S., Pracejus B., Nasir S., Al-Abri A.H., Kusky T.M. & Ghulam A., 2012. ASTER detection of chromite bearing mineralized zones in Semail Ophiolite Massifs of the northern Oman Mountains: Exploration strategy. *Ore Geology Reviews*, 44, 121–135. https://doi.org/10.1016/j.oregeorev.2011.09.010.

Sabins F.F., 1999. Remote sensing for mineral exploration. *Ore Geology Reviews*, 14, 157–183. https://doi.org/10.1016/S0169-1368(99)00007-4.

Santosh M., 2020. The Southern Granulite Terrane: A synopsis. *Episodes*, 43, 109–123. https://doi.org/10.18814/epiiugs/2020/020006.

Scott P.W., Jackson T. & Dunham A.C., 2000. Ore mineral associations and industrial minerals in the ultramafic rocks of Jamaica and Tobago. *Caribbean Journal of Earth Science*, 34, 5–16.

Sgavetti M., Pompilio L. & Meli S., 2006. Reflectance spectroscopy (0.3–2.5 μm) at various scales for bulk-rock identification. *Geosphere*, 2, 142–160. https://doi.org/10.1130/GES00039.1.

Smirnoff A., Boisvert E. & Paradis S.J., 2008. Support vector machine for 3D modelling from sparse geological information of various origins. *Computers & Geosciences*, 34, 127–143. https://doi.org/10.1016/j.cageo.2006.12.008.

Sultan M., Arvidson R.E., Sturchio N.C. & Guinness E.A., 1987. Lithologic mapping in arid regions with Landsat thematic mapper data: Meatiq dome, Egypt. *Geological Society of America Bulletin*, 99(6), 748–762.

Uthup S., Tsunogae T., Rajesh V.J., Santosh M., Takamura Y. & Tsutsumi Y., 2020. Neoarchean arc magmatism and Paleoproterozoic granulite-facies metamorphism in the Bhavani Suture Zone, South India. *Geological Journal*, 55, 3870–3895. https://doi.org/10.1002/gj.3641.

Vapnik V.N., 2000. *The Nature of Statistical Learning Theory*. 2nd ed., Statistics for Engineering and Information Science, Springer New York.

Yamaguchi Y. & Naito C., 2003. Spectral indices for lithologic discrimination and mapping by using the ASTER SWIR bands. *International Journal of Remote Sensing*, 24, 4311–4323. https://doi.org/10.1080/01431160110070320.